Journal of Elasticity
https://doi.org/10.1007/s10659-022-09936-x

An Elementary Model of Focal Adhesion Detachment and Reattachment During Cell Reorientation Using Ideas from the Kinetics of Wiggly Energies

Rohan Abeyaratne[1] · Eric Puntel[2] · Giuseppe Tomassetti[3]

Dedicated to the memory of Jerald L. Ericksen

Received: 11 July 2022 / Accepted: 15 September 2022

Abstract

A simple, transparent, two-dimensional, nonlinear model of cell reorientation is constructed in this paper. The cells are attached to a substrate by "focal adhesions" that transmit the deformation of the substrate to the "stress fibers" in the cell. When the substrate is subjected to a deformation, say an in-plane bi-axial deformation with stretches λ_1 and λ_2, the stress fibers deform with it and change their length and orientation. *In addition*, the focal adhesions can detach from the substrate and reattach to it at new nearby locations, and this process of detachment and reattachment can happen many times. In this scenario the (varying) fiber angle Θ *in the reference configuration* plays the role of an internal variable. In addition to the elastic energy of the stress fibers, the energy associated with the focal adhesions is accounted for by a wiggly energy $\epsilon a \cos \Theta/\epsilon$, $0 < \epsilon \ll 1$. Each local minimum of this energy corresponds to a particular configuration of the focal adhesions. The small amplitude ϵa indicates that the energy barrier between two neighboring configurations is relatively small, and the small distance $2\pi\epsilon$ between the local minima indicates that a focal adhesion does not have to move very far before it reattaches. The evolution of this system is studied using a gradient flow kinetic law, which is homogenized for $\epsilon \to 0$ using results from weak convergence. The results determine (*a*) a region of the λ_1, λ_2-plane in which the (referential) fiber orientation remains stuck at the angle Θ and does not evolve, and (*b*) the evolution of the orientation when the stretches move out of this region as the fibers seek to minimize energy.

✉ R. Abeyaratne
rohan@mit.edu

E. Puntel
eric.puntel@uniud.it

G. Tomassetti
giuseppe.tomassetti@uniroma3.it

1 Massachusetts Institute of Technology, Cambridge, USA

2 Università di Udine, Udine, Italy

3 Università degli Studi Roma Tre, Roma, Italy

Published online: 10 October 2022

Keywords Reorientation · Stress fibers · Detach and reattach · Wiggly energy · Internal variable · Energy minimization · Gradient flow · Weak convergence · Focal adhesions

Mathematics Subject Classification (2020) 74A15 · 74B20 · 92C05

1 Introduction

The reference configuration plays a central role in continuum solid mechanics. In the simplest settings it is a fixed (time-independent) configuration of the body with material points being identified by their position vectors in this configuration. On the other hand, many interesting physical phenomena involve time-dependent, i.e., varying, reference configurations. This is encountered for example in problems involving propagating "defects" (such as cracks, dislocations and phase boundaries): not only do the defects move when viewed from the laboratory frame (i.e. the current configuration), but, since they are associated with different material points at different times, they also move with respect to the reference configuration. A different setting in which one confronts this same issue is in surface growth, where new material points are added to the body at its boundary which therefore requires one to consider a varying set of material points, i.e., a time-dependent reference configuration.

One way in which to view the problem examined in this paper is that it is a study of a fiber-reinforced composite material in which the fiber orientation Θ *in the reference configuration* is time-dependent. Consider as a toy problem a single fiber attached at its two ends to a substrate. As the substrate deforms, so does the fiber. Now suppose that in addition to the substrate deformation, the attachments between the fiber and substrate can detach and then reattach at some new points on the substrate, and that this process can continue until the fiber has reached a new preferred length and orientation. Our goal is to model a system undergoing such a process of reorientation.

This problem is motivated by the phenomenon of reorientation in cell biology, e.g., [9], [10], [11], [12], [17], [23]. In this setting, the stress fibers in the cytoskeleton of the cell are attached to a substrate (the extra-cellular matrix) by "focal adhesions" that transmit force between the substrate and the cell. When the substrate is deformed, say cyclically,[1] the stress fibers reorient themselves during which process the focal adhesions continually detach and reattach at different nearby sites until they eventually reach a steady state. The details of this process, and the final fiber orientation, depend on the amplitude, frequency and bi-axiality ratio of the loading, e.g., [6], [13], [17]; see discussion surrounding equation (B.8) in Appendix B.

In addition to the experimental work described in the aforementioned references, several theoretical studies of such systems have been carried out. A few from among them are the following: an isotropic linear elasticity model by Faust et al. [10]; an anisotropic linear elasticity model by Livne et al. [17]; continuum mechanical models based on nonlinear elasticity by Melnik and Goriely [20], Ciambella and Nardinocchi [8], Ciambella et al. [7], Lucci and Preziosi [19]; a viscoelastic model by Lucci, Giverso and Preziosi [18]; a coexistent phase nonlinearly elastic model by Lazopoulos and Stamenovic [16], Lazopoulos and Pirentis [15]; and so on. Ciambella and Nardinocchi [8] point out that similar reorientation occurs in other physical systems such as liquid crystals and liquid crystal elastomers. We also draw attention to the micromechanics based three-dimensional model developed

[1] In this context, such periodic loading occurs, for example, in the lungs due to breathing, arteries due to pulsating blood flow, and cardiac muscles due to the beating heart.

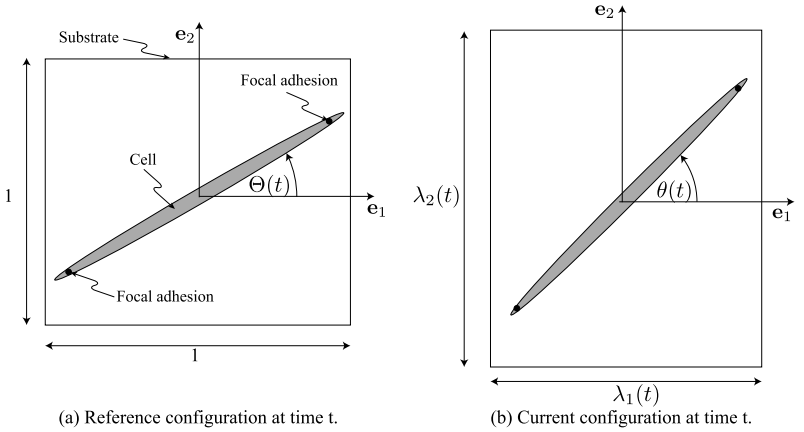

(a) Reference configuration at time t. (b) Current configuration at time t.

Fig. 1 A cartoon of the system. The "cell" is attached at its two ends to the substrate by a pair of "focal adhesions". During a loading process the substrate is subjected to stretches $\lambda_1(t)$ and $\lambda_2(t)$ in the respective directions $\mathbf{e}_1$ and $\mathbf{e}_2$ where t is time, and this deformation is transmitted to the cell by the focal adhesions. (a) In the reference configuration the cell makes an angle $\Theta(t)$ at time t with the direction $\mathbf{e}_1$. The referential angle $\Theta(t)$ is time-dependent because the focal adhesions can detach and then reattach to different points of the substrate. (b) In the current configuration the cell makes an angle $\theta(t)$ with $\mathbf{e}_1$

by Vigliotti et al. [24], as well as the study of the reorientation of cells overlying grooved substrates, Ristori et al. [22].

The *first goal* of the present paper is to construct a simple, transparent, two-dimensional, nonlinear model that is essentially equivalent to the aforementioned nonlinearly elastic models [8], [19] but whose construction by-passes the complexities (as well as the generalities, rigor and elegance) of continuum mechanics.

In many problems involving a changing reference configuration, one introduces an internal variable to characterize an evolving feature of that configuration, e.g., the position of a crack-tip or the surface describing a phase boundary. A change in the internal variable leads to energy dissipation and through this one can identify a work-conjugate driving force (sometimes referred to as a configurational force). In thermodynamic equilibrium, the driving force vanishes, a concept closely related to the minimization of energy. When the system is not in equilibrium, the internal variable evolves according to a kinetic law relating the driving force to the rate-of-change of the internal variable (and possibly other variables), e.g., Callen [5] and Kestin [14]. This is the approach we follow.

We characterize the mechanical response of a cell by an energy function $W(\lambda_1, \lambda_2, \Theta)$ where λ_1 and λ_2 are the in-plane stretches of the substrate that are transmitted to the cell via the focal adhesions, and the internal variable Θ is the angle of orientation of the cell in the reference configuration; see Fig. 1 for a schematic depiction of the system. While we illustrate our approach using an energy of the form $W(\Lambda)$ where $\Lambda(\lambda_1, \lambda_2, \Theta)$ is the stretch along the fibers, our approach is not limited to such energies. During a (slow) nonequilibrium process with $\lambda_1 = \lambda_1(t)$, $\lambda_2 = \lambda_2(t)$, $\Theta = \Theta(t)$, the dissipation-rate is the difference between the rate of working and the rate of increase of stored energy:

$$\mathbb{D} := \sigma_1 \dot{\lambda}_1 + \sigma_2 \dot{\lambda}_2 - \frac{d}{dt} W(\lambda_1(t), \lambda_2(t), \Theta(t)) = -\frac{\partial W}{\partial \Theta} \dot{\Theta} \geq 0, \tag{1}$$

where $\sigma_\alpha = \partial W/\partial\lambda_\alpha$ is a Piola stress component. Observe that the dissipation-rate vanishes if the internal variable Θ is constant. The dissipation-rate can be written as

$$\mathbb{D} = \mathfrak{f}\,\dot{\Theta} \geq 0 \qquad \text{where} \quad \mathfrak{f} := -\frac{\partial W}{\partial \Theta} \tag{2}$$

is the *driving force* conjugate to $\dot{\Theta}$. In thermodynamic equilibrium $\mathfrak{f} = 0$:

$$\frac{\partial W}{\partial \Theta} = 0.$$

The evolution of the system when it is not in equilibrium is taken to be governed by a kinetic law $\dot{\Theta} = \mathsf{V}(\mathfrak{f})$ where the kinetic response function V obeys $\mathsf{V}(\mathfrak{f})\mathfrak{f} \geq 0$ required by the dissipation inequality $\mathbb{D} \geq 0$. The simplest example of such a kinetic law is a gradient flow,

$$\mathsf{m}\,\dot{\Theta} = \mathfrak{f},$$

which is a linear relation between $\dot{\Theta}$ and the conjugate driving force $\mathfrak{f}$, the constant parameter $\mathsf{m} > 0$ being the mobility.

The *second and in fact principal goal* of the present paper is to model the detachment/reattachment process using a wiggly energy. During reorientation, a focal adhesion along a stress fiber detaches from the substrate and reattaches at a new, nearby, location. This process of detachment and reattachment repeats continually as the fiber reorients. This suggests that the energy associated with a focal adhesion has many local minima, each corresponding to a particular configuration of the focal adhesion, with some amount of energy required to move it from one local minimum to the next. To account for this in as simple a way as possible, we supplement the energy considered above with an additional wiggly energy $a\epsilon\cos\Theta/\epsilon$ associated with the focal adhesions. The distance between the energy wells of this periodic energy, and its amplitude (the energy barrier), both scale with the small parameter ϵ. The small amplitude indicates that only a small amount of energy is needed to crossover from one energy-well to the next, and the smallness of the distance between local minima indicate that focal adhesions do not displace far before they reattach. Thus we next consider the energy

$$W_\epsilon(\Theta;\lambda_1,\lambda_2) = W(\Theta;\lambda_1,\lambda_2) + a\epsilon\cos\Theta/\epsilon, \quad a > 0,\ 0 < \epsilon \ll 1. \tag{3}$$

The driving force associated with W_ϵ is

$$\mathfrak{f}_\epsilon(\Theta;\lambda_1,\lambda_2) := -\frac{\partial W_\epsilon}{\partial\Theta}(\Theta;\lambda_1,\lambda_2) = \mathfrak{f}(\Theta;\lambda_1,\lambda_2) + a\sin(\Theta/\varepsilon);$$

observe that while the wiggly energy $\to 0$ as $\epsilon \to 0$ the associated driving force *does not*. If the evolution obeys a gradient flow kinetic law then

$$\mathsf{m}\,\dot{\Theta}_\epsilon = -\frac{\partial W_\epsilon}{\partial\Theta}(\Theta_\epsilon;\lambda_1,\lambda_2).$$

Given the loading $\lambda_1(t)$, $\lambda_2(t)$ and the initial orientation $\Theta_\epsilon(0)$, this kinetic equation is be solved for $\Theta_\epsilon(t)$. However, we are not interested in this detailed (exact) solution $\Theta_\epsilon(t)$ that accounts for each attachment and detachment of a focal adhesion. It is the *effective kinetic law* governing the effective orientation that is of interest and this leads us to homogenize the preceding differential equation using the results of Abeyaratne, Chu and James [1], [2]. As

we shall show, this determines a region of the λ_1, λ_2-plane on which fibers do not reorient. The boundary of this region is the threshold for reorientation, with the orientation evolving according to the effective kinetic law when the stretches lie outside this region. This is consistent with the qualitative observations reported by Faust et al. [10]. We have not found quantitative information on this phenomenon in the literature, and it would be important to compare our predictions with such measurements.

Given the minimalistic nature of our model, the internal variable Θ need not represent the orientation of a family of fibers. A model like the one we develop could possibly be used to study other physical systems, for example, friction, though one must of course choose a function $W_\epsilon(\Theta; \lambda_1, \lambda_2)$ appropriate for that system.

The rest of this paper is organized as follows: the basic problem is described in Sect. 2. Then in Sect. 3 we examine the equilibrium configurations of the system and their stability. The evolution of the system when it is out of equilibrium is studied in Sect. 4, and in Sect. 5 we incorporate the kinetics of attachment and detachment through a wiggly energy.

2 Preliminaries

We imagine a cell to be a slender ellipse-like two-dimensional object overlying a substrate. Each cell is attached to the substrate, the substrate being the loading device that applies a deformation to the cell. The substrate is subjected to a homogeneous deformation with gradient

$$\mathbf{F}(t) = \lambda_1(t)\mathbf{e}_1 \otimes \mathbf{e}_1 + \lambda_2(t)\mathbf{e}_2 \otimes \mathbf{e}_2 + \lambda_3(t)\mathbf{e}_3 \otimes \mathbf{e}_3 \tag{4}$$

at time t, where the λ_i's are the principal stretches, the principal directions $\{\mathbf{e}_1, \mathbf{e}_2, \mathbf{e}_2\}$ are fixed, and the cells lie in the plane spanned by $\mathbf{e}_1$ and $\mathbf{e}_2$.

We assume the "stress fibers" in a cell to be oriented in the direction of its major axis. Though a cell is attached to the substrate, its points of attachment can change and so its orientation *in the reference configuration is time-dependent* in general. In the setting of interest here, there are two families of cells with the associated stress fibers oriented at angles[2] $\pm\Theta(t)$ in the reference configuration with respect to the direction $\mathbf{e}_1$. With no loss of generality we take $\Theta \in [0, \pi/2]$. The unit vectors defining the stress fiber directions (in the reference configuration) are

$$\mathbf{m}_{\mathrm{R}}(t) = \cos\Theta(t)\,\mathbf{e}_1 + \sin\Theta(t)\,\mathbf{e}_2, \quad \mathbf{m}'_{\mathrm{R}}(t) = \cos\Theta(t)\,\mathbf{e}_1 - \sin\Theta(t)\,\mathbf{e}_2. \tag{5}$$

In the *deformed* configuration the stress fibers make angles $\pm\theta(t)$ with the $\mathbf{e}_1$-direction given by

$$\tan\theta = \frac{\lambda_2}{\lambda_1}\tan\Theta. \tag{6}$$

If the cell was attached to fixed points of the substrate, then Θ would be constant though θ would vary with t when the deformation was time-dependent.

[2] Livne et al. [17] say they observe two angles, one the mirror image of the other. Hence, like Livne et al. [17] and Ciambella and Nardinocchi [8] we take the fiber angles to be $\pm\Theta$. In contrast, Lucci and Preziosi [19] take them to be Θ and $\Theta + \pi/2$.

In what follows, the stretches Λ_1 and Λ_2 in the directions of the major and minor axes of the ellipse-like cell, i.e., the stress fiber direction and the direction perpendicular to it, will play a central role. They are given by

$$\Lambda_1 = \sqrt{\lambda_1^2 \cos^2\Theta + \lambda_2^2 \sin^2\Theta}, \quad \Lambda_2 = \sqrt{\lambda_1^2 \sin^2\Theta + \lambda_2^2 \cos^2\Theta}. \tag{7}$$

We note in passing that when viewed from the continuum theory of nonlinear elasticity, the anisotropic invariants $I_4 := |\mathbf{F}\mathbf{m}_R|^2$ and $I_6 := |\mathbf{F}\mathbf{m}'_R|^2$ can be readily shown using (4), (5) and $(7)_1$ to be

$$I_4 = I_6 = \Lambda_1^2. \tag{8}$$

If the cell can be treated as being elastic and isotropic, then its energy can be expressed as a function of λ_1 and λ_2. However, due to the preferred orientation induced by the stress fibers, the response is anisotropic and the energy will be a function of the fiber orientation Θ as well:

$$W = \widehat{W}(\lambda_1, \lambda_2, \Theta); \tag{9}$$

see, for example, Ogden [21]. Since we model the substrate as a hard loading device that applies a prescribed deformation, the energy of the substrate does not enter the model.

Given the stretches λ_1 and λ_2, we are first interested in the equilibrium fiber orientations that minimize the energy $\widehat{W}(\lambda_1, \lambda_2, \Theta)$, i.e., the angles Θ given by

$$\frac{\partial \widehat{W}}{\partial \Theta} = 0, \quad \left.\frac{\partial^2 \widehat{W}}{\partial \Theta^2}\right|_{\text{equilibrium}} > 0. \tag{10}$$

Some authors have assumed that, instead of minimizing the energy, the fibers orient themselves in the directions of minimum strain or minimum stress; see references and discussion in Livne et al. [17].

During a (slow) nonequilibrium process with $\lambda_1 = \lambda_1(t)$, $\lambda_2 = \lambda_2(t)$, $\Theta = \Theta(t)$, the local dissipation-rate $\mathbb{D}$ is the difference between the rate of working and the rate of increase of stored energy given by (1). From the alternate expression $(2)_1$ for $\mathbb{D}$ we identify

$$\mathfrak{f} = -\frac{\partial \widehat{W}}{\partial \Theta}, \tag{11}$$

to be the driving force conjugate to the orientation Θ; see, e.g., [3], [4], [5], [14]. Observe that $\mathfrak{f} = 0$ in equilibrium.

We assume that when it is out of equilibrium, the fiber orientation evolves according to a gradient flow, i.e., a linear kinetic relation between the rate of change of the referential orientation $\dot{\Theta}$ and the driving force $\mathfrak{f}$:

$$\mu\tau\,\dot{\Theta} = -\frac{\partial \widehat{W}}{\partial \Theta}. \tag{12}$$

For convenience we have introduced the constant $\mu > 0$ here which is a parameter that appears in $\widehat{W}$ and has the dimension of $\widehat{W}$. The constant $\tau > 0$ then has the dimension of time and characterizes the rate at which the cells reorient themselves as they evolve towards equilibrium. The term $\mathsf{m} := \mu\tau > 0$ is thus the mobility whose positivity ensures that the dissipation-rate is nonnegative.

3 Equilibrium and Stability

Though our model is not limited to the following energy function, it is convenient for purposes of illustration to consider an energy of the form[3]

$$\widehat{W}(\lambda_1, \lambda_2, \Theta) = W(\Lambda_1), \tag{13}$$

where Λ_1 is the stretch in the stress fiber direction introduced previously in $(7)_1$. In the context of the continuum theory of nonlinear elasticity, such an energy corresponds, for example, to a strain energy function that is the sum of an isotropic part (a function of the principal scalar invariants I_1, I_2, I_3 that are independent of Θ and so has been omitted since it does not affect our analysis here) and an anisotropic part of the form $\overline{W}(I_4, I_6)$ where the anisotropic invariants I_4 and I_6 were given previously in (8). We assume the following mild restrictions on $W(\Lambda)$:

$$W'(1) = 0, \quad W''(1) > 0; \quad W'(\Lambda) \begin{cases} > 0 & \text{for} \quad \Lambda > 1, \\ < 0 & \text{for} \quad 0 < \Lambda < 1. \end{cases} \tag{14}$$

Note in particular that $\Lambda = 1$ is the *unique zero* of the function $W'(\Lambda)$.

The first and second derivatives of $\widehat{W}$ with respect to Θ are

$$\frac{\partial \widehat{W}}{\partial \Theta} = \frac{W'(\Lambda_1)}{2\Lambda_1}(\lambda_2^2 - \lambda_1^2)\sin 2\Theta, \tag{15}$$

$$\frac{\partial^2 \widehat{W}}{\partial \Theta^2} = \frac{\Lambda_1 W''(\Lambda_1) - W'(\Lambda_1)}{4\Lambda_1^3}(\lambda_1^2 - \lambda_2^2)^2 \sin^2 2\Theta - \frac{W'(\Lambda_1)}{\Lambda_1}(\lambda_1^2 - \lambda_2^2)\cos 2\Theta. \tag{16}$$

Motivated by the experiments of Livne et al. [17], we will be interested in equilibrium configurations with

$$\lambda_1 \geq 1 \geq \lambda_2 > 0, \tag{17}$$

and so in particular shall not consider equilibria in which[4] $\lambda_1 = \lambda_2$ except for the trivial one $\lambda_1 = \lambda_2 = 1$.

According to $(10)_1$, (15) and $\lambda_1 \neq \lambda_2$ the equilibrium configurations are given by

$$W'(\Lambda_1)\sin 2\Theta = 0, \tag{18}$$

which yields

$$\Theta = 0, \quad \Theta = \frac{\pi}{2}, \quad \Theta = \Theta_{\text{eq}}. \tag{19}$$

Here Θ_{eq} is the *unique* angle in $[0, \pi/2]$ corresponding to $W'(\Lambda_1) = 0$, which by (14) corresponds to $\Lambda_1 = 1$, and therefore by $(7)_1$ is given by

$$\cos^2 \Theta_{\text{eq}} = \frac{1 - \lambda_2^2}{\lambda_1^2 - \lambda_2^2}. \tag{20}$$

[3] Lucci and Preziosi [19] say that the stiffness in the direction of the stress fibers is 2-10 times greater than in the direction normal to them.

[4] Wang et al. [12] say there is no preferred orientation when $\lambda_1 = \lambda_2$ which is consistent with (15) and (16).

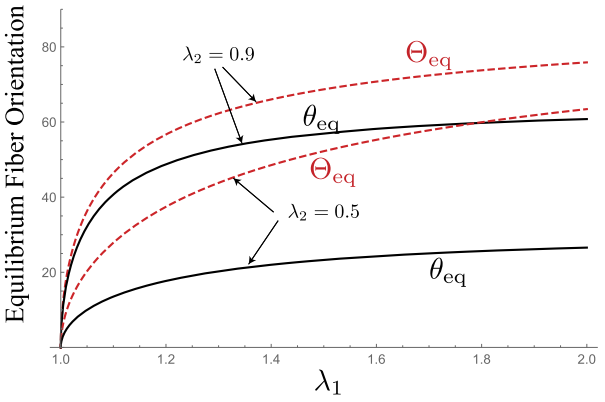

Fig. 2 The equilibrium fiber orientations $\Theta_{\rm eq}$ and $\theta_{\rm eq}$ (in the reference and current configurations respectively) versus the stretch λ_1 at different constant values of λ_2. Observe that $\Theta_{\rm eq} \to \pi/2$ while $\theta_{\rm eq} \to \cos^{-1}\sqrt{1-\lambda_2^2}$ as $\lambda_1 \to \infty$ in accordance with (20) and (21). It is $\theta_{\rm eq}$ that is observed in the laboratory

In view of the inequalities in (17), equation (20) defines a real angle $\Theta_{\rm eq}$.

The fiber orientation $\theta_{\rm eq}$ in the deformed configuration is given by (6) and (20) to be

$$\cos^2\theta_{\rm eq} = \frac{1-\lambda_2^2}{\lambda_1^2-\lambda_2^2}\lambda_1^2. \tag{21}$$

It is worth noting that it is $\theta_{\rm eq}$ (not $\Theta_{\rm eq}$) that is *observed* in the laboratory. For example if the stretch λ_1 increases monotonically from $\lambda_1 = 1$ with $\lambda_2 < 1$ held constant, the equilibrium angle $\theta_{\rm eq}$ in the current configuration increases from 0 to $\cos^{-1}\sqrt{1-\lambda_2^2}$, whereas the angle $\Theta_{\rm eq}$ in the reference configuration increases from 0 to $\pi/2$ (no matter what the value of λ_2). If the stretch λ_2 is held constant at $\lambda_2 = 1$, then $\theta_{\rm eq} = \Theta_{\rm eq} = \pi/2$ for all $\lambda_1 > 1$; and similarly $\theta_{\rm eq} = \Theta_{\rm eq} = 0$ for $\lambda_1 = 1$ and $\lambda_2 < 1$. Graphs of $\Theta_{\rm eq}$ and $\theta_{\rm eq}$ versus λ_1 are shown in Fig. 2.

To study the stability of these equilibria we evaluate the second derivatives of $\widehat{W}$ at each equilibrium configuration which from (16), (19) and (20) lead to

$$\left.\frac{\partial^2\widehat{W}}{\partial\Theta^2}\right|_{\Theta=0} = -\frac{W'(\lambda_1)}{\lambda_1}(\lambda_1^2-\lambda_2^2), \qquad \left.\frac{\partial^2\widehat{W}}{\partial\Theta^2}\right|_{\Theta=\pi/2} = \frac{W'(\lambda_2)}{\lambda_2}(\lambda_1^2-\lambda_2^2), \tag{22}$$

$$\left.\frac{\partial^2\widehat{W}}{\partial\Theta^2}\right|_{\Theta=\Theta_{\rm eq}} = W''(1)(\lambda_1^2-1)(1-\lambda_2^2). \tag{23}$$

Keeping (14) and (17) in mind, we conclude that the equilibrium configurations $\Theta = 0$ and $\Theta = \pi/2$ are unstable (they correspond to local maxima of $\widehat{W}(\lambda_1, \lambda_2, \cdot)$), while the configuration $\Theta = \Theta_{\rm eq}$ is stable (it corresponds to a local minimum of $\widehat{W}(\lambda_1, \lambda_2, \cdot)$). Figure 3 schematically depicts the variation of $\widehat{W}$ with Θ at fixed λ_1, λ_2.

It is worth remarking that the preceding results on the equilibrium configurations and their stability do not depend on any particular choice of the energy $W(\Lambda_1)$.

Some detailed results pertaining to the equilibrium fiber orientation, and how they compare with the results of others, can be found in Appendix A.

4 Slow Dynamic Evolution: Illustration

From hereon we will primarily focus on the angle $\Theta(t)$ in the reference configuration. The corresponding angle $\theta(t)$ in the current configuration can always be calculated using (6).

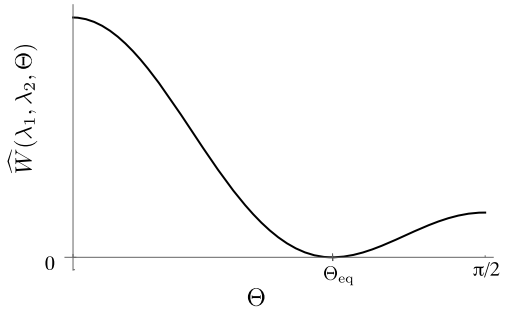

Fig. 3 Energy $\widehat{W}$ versus orientation Θ at fixed values of the principal stretches. The figure has been drawn for the particular energy $W(\Lambda_1) = \frac{\mu}{2}(\Lambda_1^2 - 1)^2$ with $\lambda_1 = 1.2$, $\lambda_2 = 0.9$. The key characteristics of the curve do not depend on this particular choice of $W(\Lambda_1)$

According to (12) and (15), in a slow nonequilibrium process the fiber orientation evolves according to the linear gradient flow kinetic relation

$$\mu\tau\,\dot{\Theta} = -\frac{\partial W}{\partial \Theta} = \frac{W'(\Lambda_1)}{2\Lambda_1}(\lambda_1^2 - \lambda_2^2)\sin 2\Theta. \tag{24}$$

To illustrate the details of this evolution, consider the particular energy function

$$W(\Lambda_1) = \frac{1}{2}\mu(\Lambda_1^2 - 1)^2, \quad \mu > 0, \tag{25}$$

where the elastic modulus μ is a constant. This corresponds, for example, to the energy $W = \frac{1}{2}\mu_4(I_4 - 1)^2 + \frac{1}{2}\mu_6(I_6 - 1)^2$ of nonlinear elasticity theory where I_4 and I_6 are the two anisotropic invariants introduced previously. This is in fact precisely the model considered by Melnik and Goriely [20] and one of the models used by Ciambella and Nardinocchi [8]; it is also closely related to a special case of a model considered by Lucci and Preziosi [19]. From $(7)_1$ and (25) this energy can be written explicitly as

$$\begin{aligned}\widehat{W}(\lambda_1, \lambda_2, \Theta) &= \frac{\mu}{8}\Big[(\lambda_1^2 - \lambda_2^2)^2\cos^2 2\Theta \;+\; 2(\lambda_1^2 - \lambda_2^2)(\lambda_1^2 + \lambda_2^2 - 2)\,\cos 2\Theta \\ &\quad +\; (\lambda_1^2 + \lambda_2^2 - 2)^2\Big].\end{aligned} \tag{26}$$

Figure 3 presented earlier, where we plotted $\widehat{W}$ versus Θ at fixed λ_1 and λ_2, pertained to the particular energy (26).

The evolution equation (24), (25) can now be written as

$$\tau\dot{\Theta} = F(\Theta; \lambda_1, \lambda_2), \tag{27}$$

where the (scaled) driving force[5] F is

$$F(\Theta; \lambda_1, \lambda_2) = \big[A(\lambda_1, \lambda_2)\cos^2\Theta - B(\lambda_1, \lambda_2)\big]\sin 2\Theta, \tag{28}$$

with

$$A(\lambda_1, \lambda_2) = (\lambda_1^2 - \lambda_2^2)^2, \quad B(\lambda_1, \lambda_2) = (\lambda_1^2 - \lambda_2^2)(1 - \lambda_2^2). \tag{29}$$

[5]Note that $F = \mathfrak{f}/\mu$ where $\mathfrak{f}$ is the driving force introduced previously in (11).

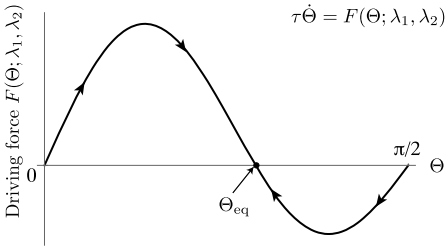

Fig. 4 Driving force F versus Θ at fixed λ_1, λ_2 according to (28), (29). When $\Theta \in (0, \Theta_{\rm eq})$ the driving force is positive and $\Theta(t)$ will increase towards $\Theta_{\rm eq}$; whereas if $\Theta \in (\Theta_{\rm eq}, \pi/2)$ the driving force is negative and $\Theta(t)$ will decrease towards $\Theta_{\rm eq}$. This is depicted by the arrows in the figure. The figure has been drawn for $\lambda_1 = 1.5, \lambda_2 = 0.5$

The evolution equations (27), (28), (29) coincide with equations (3.39), (4.42) of Ciambella and Nardinocchi [8].

Evolution according to the kinetic relation (27) depends on the characteristics of the driving force F. With a prime denoting differentiation with respect to Θ, one can show that F has the following properties: $F(0;\lambda_1,\lambda_2) = 0$, $F'(0;\lambda_1,\lambda_2) > 0$, $F(\pi/2;\lambda_1,\lambda_2) = 0$, $F'(\pi/2;\lambda_1,\lambda_2) > 0$, $F(\Theta_{\rm eq};\lambda_1,\lambda_2) = 0$, $F'(\Theta_{\rm eq};\lambda_1,\lambda_2) < 0$. Moreover, one can verify that $F(\cdot;\lambda_1,\lambda_2)$ has a unique local maximum in $(0, \Theta_{\rm eq})$ and a unique local minimum in $(\Theta_{\rm eq}, \pi/2)$. Therefore the graph of the driving force $F(\Theta;\lambda_1,\lambda_2)$ versus Θ at any fixed λ_1, λ_2 with $\lambda_1 > 1 > \lambda_2 > 0$ is as shown in Fig. 4. The function $F(\cdot;\lambda_1,\lambda_2)$ vanishes at $\Theta = 0, \pi/2$ and $\Theta_{\rm eq}$; is positive on $(0, \Theta_{\rm eq})$; and negative on $(\Theta_{\rm eq}, \pi/2)$. Moreover, when Θ increases from 0, the curve rises to a local maximum on $(0, \Theta_{\rm eq})$, then falls to a local minimum in $(\Theta_{\rm eq}, \pi/2)$, before rising again. Though the figure shows the height of the peak to be larger than the depth of the valley, this is not always true – it depends on the values of λ_1, λ_2.

The Θ, F-plane shown in Fig. 4 is in fact the phase plane for the ordinary differential equation (27) (at fixed λ_1, λ_2). The three intersection points of the graph of F with the horizontal axis are equilibrium (stationary) points of $\tau\dot{\Theta} = F(\Theta;\lambda_1,\lambda_2)$. We see from Fig. 4 that whenever $\Theta(t) \in (0, \Theta_{\rm eq})$, the driving force is positive. Consequently $\dot{\Theta} > 0$ and $\Theta(t)$ will increase towards $\Theta_{\rm eq}$. On the other hand if $\Theta(t) \in (\Theta_{\rm eq}, \pi/2)$, the driving force is negative, thus $\dot{\Theta} < 0$, and so $\Theta(t)$ will decrease towards $\Theta_{\rm eq}$. This is depicted by the arrows in the figure. Thus trajectories leave the equilibrium points $(0, 0)$ and $(\pi/2, 0)$, and therefore they are unstable, whereas trajectories enter the stable equilibrium point $(\Theta_{\rm eq}, 0)$. This is consistent with the energy sketched in Fig. 3 which has local maxima at $\Theta = 0$ and $\pi/2$ and a local minimum at $\Theta_{\rm eq}$.

Given $\lambda_1(t)$, $\lambda_2(t)$ and $\Theta(0)$, equation (27) is to be solved for $\Theta(t)$. Figure 5 displays the predicted response when the specimen is subjected to the monotonic loading described in the figure caption. One can verify from (20) that the equilibrium fiber orientation corresponding to the initial conditions is $\Theta_{\rm eq} = 0^o$, and since this is smaller than the initial fiber orientation $\Theta(0) = 50^o$, the curves decline at the initial instant as $\Theta(t)$ starts to evolve towards $\Theta_{\rm eq}$. However, when the value of the stretch $\lambda_1(t)$ becomes sufficiently large, the sign of $\dot{\Theta}$ as given by (27) becomes positive and the curves turns around and rise. This is most apparent in the curve corresponding to $\varepsilon = 1/25$ where the loading is very slow. Some additional results can be found in Appendix B.

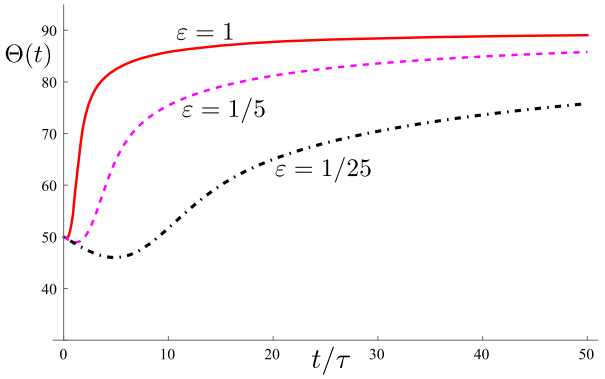

Fig. 5 Fiber orientation $\Theta(t)$ versus time t/τ according to the kinetic relation (27), (28), (29). The figure has been drawn for the monotonic loading $\lambda_1 = 1 + 0.5\, t/T$ with $\lambda_2 = 0.9$ and $\Theta(0) = 50^o$. The parameter $\varepsilon = \tau/T$ is the ratio between the kinetic and loading timescales τ and T respectively. Observe that $\lambda_1(t) \to \infty$ as $t \to \infty$ so that in accordance with (20), $\Theta(t) \to \pi/2$ in this limit; see also the upper dashed curve in Fig. 2

5 Accounting for the Energy of Detachment/Attachment

For the reasons described in the paragraph containing (3) in the introduction (Sect. 1), we now consider the energy

$$W_\epsilon(\Theta; \lambda_1, \lambda_2) = W(\Theta; \lambda_1, \lambda_2) + a\epsilon \cos\Theta/\epsilon, \quad a > 0,\ 0 < \epsilon \ll 1, \tag{30}$$

where W is given by (26) and we have dropped the hat from W. The energy $a\epsilon \cos\Theta/\epsilon$ is associated with the focal adhesions. Each of its local minima corresponds to a particular configuration of the focal adhesions. The distance between the energy wells of this periodic energy, and its amplitude (the energy barrier), both scale with ϵ. The small amplitude indicates that only a small amount of energy is needed to crossover from one energy-well to the next, and the smallness of the distance between local minima indicates that focal adhesions do not displace far before they reattach.

For small ϵ, the energy $a\epsilon \cos\Theta/\epsilon$ has a periodic array of many energy wells (local minima) in the interval $[0, \pi/2]$. On the other hand a function such as $\alpha\Theta + a\epsilon \cos\Theta/\epsilon$, $\alpha > 0$, will have local minima only if the slope α of the linear term is sufficiently small. For large α, the curvature of the combined function will keep changing without it having any local minima. With this as background, recall from Fig. 3 that the graph of W versus Θ is flat (has zero slope) at $\Theta = 0$, Θ_{eq} and $\pi/2$. When $a\epsilon \cos\Theta/\epsilon$ is added to W, the combined energy W_ϵ will therefore inherit local minima in the vicinity of these three extremal points. This can be seen in Fig. 6 where the top (blue) curve corresponds to W and the middle (black) to W_ϵ. Ignore the bottom (red) curve for now. For clarity, the curves have been shifted slightly in the vertical direction. The system can get stuck (be in metastable equilibrium) in any one of these energy wells. Away from $\Theta = 0$, Θ_{eq} and $\pi/2$ the combined energy may have no local minima and the system cannot be in equilibrium there.

The driving force associated with W_ϵ is

$$F_\epsilon(\Theta; \lambda_1, \lambda_2) := -\frac{\partial W_\epsilon}{\partial \Theta}(\Theta; \lambda_1, \lambda_2) = F(\Theta; \lambda_1, \lambda_2) + a \sin(\Theta/\varepsilon), \tag{31}$$

and we assume that the fiber orientation obeys the linear gradient flow kinetic law

$$\tau\, \dot{\Theta}_\epsilon = -\frac{\partial W_\epsilon}{\partial \Theta}(\Theta_\epsilon; \lambda_1, \lambda_2). \tag{32}$$

Given $\lambda_1(t)$, $\lambda_2(t)$ and $\Theta_\epsilon(0)$, the kinetic equation (32) can be solved for $\Theta_\epsilon(t)$. However we are not interested in this detailed (exact) solution $\Theta_\epsilon(t)$ that accounts for each attachment

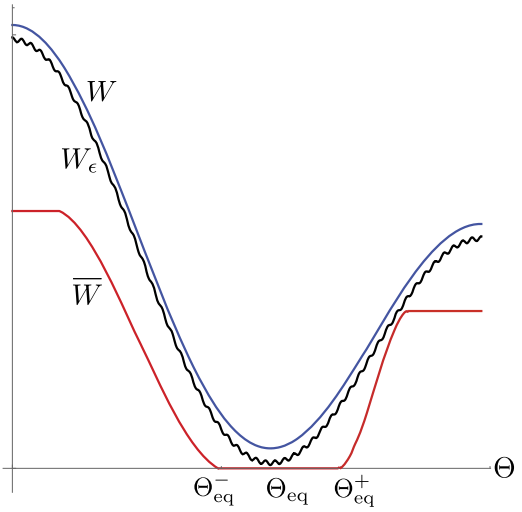

Fig. 6 Plots of the energy functions W (top), W_ϵ (middle) and $\overline{W}$ (bottom) versus Θ. For clarity, the curves have been shifted vertically

and detachment of the focal adhesions. It is the *effective kinetic law* governing the effective orientation $\Theta(t)$ that is of interest. This leads us to homogenize $\Theta_\epsilon(t)$.

Before presenting the result of homogenization, it is helpful to gain some insight[6] into what we might expect the result to look like. The response predicted by (32) depends on the characteristics of the driving force F_ϵ. Figure 7 shows a graph of $F_\epsilon(\Theta;\lambda_1,\lambda_2)$ versus Θ according to (32), (31), (28), (29), for the particular choice of parameter values given in the caption. This is essentially the phase plane for the differential equation $\tau\,\dot\Theta_\epsilon(t) = F_\epsilon(\Theta_\epsilon(t);\lambda_1,\lambda_2)$ and all motions follow the curve shown. This curve has many oscillations. More importantly, it crosses the horizontal axis at several points and therefore the differential equation (32) has many equilibrium (stationary) points. Figure 7 should be compared with Fig. 4 where we showed the driving force F without the wiggly energy.

If the process of fiber reorientation starts at any point in Fig. 7 above the horizontal axis, the driving force is positive and so $\dot\Theta_\epsilon$ will also be positive; thus the fiber will reorient towards the nearest equilibrium point to the right of the starting point. Thus a process starting at,[7] say, C will evolve all the way to D. On the other hand a process starting at A will evolve slightly before getting stuck at B.

Likewise, if the process of fiber reorientation starts at any point below the horizontal axis, the driving force is negative, $\dot\Theta_\epsilon$ is therefore also negative, and the fiber will reorient towards the nearest equilibrium point to the left of the starting point. Thus if one starts at F, reorientation occurs all the way to E, but starting at G leads to just a little change in orientation before getting stuck at H.

Thus many initial conditions lead eventually to the equilibrium points D and E, and in this sense one might speak of the single equilibrium point $\Theta_{\rm eq}$ (in the case without the wiggly energy) having bifurcated into the two equilibrium points D and E (or perhaps the family of equilibrium points between D and E).

On the other hand starting very near either end or the middle in Fig. 7 leads to very little evolution before the system gets stuck. The number of equilibrium points – the intersection points of the driving force curve with the horizontal axis – increases as $\epsilon \to 0$ eventually

[6] Throughout the following discussion we shall hold the principal stretches fixed.

[7] See the caption in Fig. 7 for how a label such as "C" relates to the dot vertically above or below it.

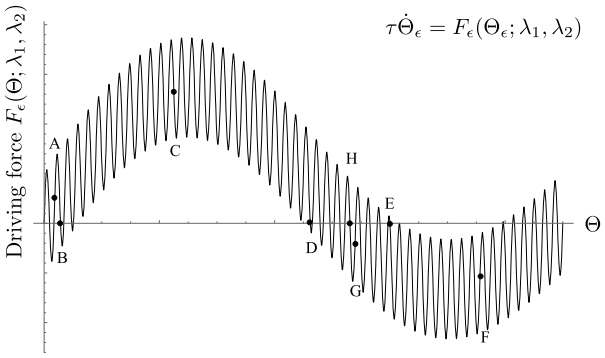

Fig. 7 Driving force F_ϵ versus Θ at fixed λ_1, λ_2 according to (28), (29), (31). This should be compared with the graph of F shown in Fig. 4. A label such as "A" refers to the dot vertically above or below it in Fig. 7. Trajectories that start at C and F evolve all the way to D and E respectively. On the other hand trajectories that start at A and G evolve just a little before getting stuck at B and H respectively. The figure has been drawn for $\lambda_1 = 1.5$, $\lambda_2 = 0.5$, $\epsilon = 0.005$ and $a = 0.5$

filling up three segments of the horizontal axis on which no evolution occurs at all, one near $\Theta = 0$, another near $\Theta = \pi/2$ and the third near $\Theta = \Theta_{\text{eq}}$.

As mentioned previously, we are not interested in the detailed solutions $\Theta_\epsilon(t)$ of the kinetic law (32) that we have just been discussing. It is the *effective kinetic law* governing the effective orientation $\Theta(t)$ that is of interest. Using weak convergence methods Abeyaratne, Chu and James [1], [2] have shown that $\Theta_\epsilon(t) \to \Theta(t)$ uniformly, where $\Theta(t)$ obeys the gradient flow

$$\tau\,\dot{\Theta} = -\frac{\partial \overline{W}}{\partial \Theta}(\Theta;\lambda_1,\lambda_2), \tag{33}$$

with the effective driving force being

$$-\frac{\partial \overline{W}}{\partial \Theta} = \begin{cases} +\sqrt{[F(\Theta;\lambda_1,\lambda_2)]^2 - a^2}, & F(\Theta;\lambda_1,\lambda_2) > a, \\ 0, & -a \le F(\Theta;\lambda_1,\lambda_2) \le a, \\ -\sqrt{[F(\Theta;\lambda_1,\lambda_2)]^2 - a^2}, & F(\Theta;\lambda_1,\lambda_2) < -a. \end{cases} \tag{34}$$

We refer the reader to [1], [2] for a proof of this result.

From (33) and (34) we see that the fiber orientation does not evolve (and therefore remains stuck at the value Θ) when $-a \le F(\Theta;\lambda_1,\lambda_2) \le a$. Thus a is a measure of the critical amount of adhesion needed for focal adhesions to detach from the substrate. The region of the λ_1, λ_2-plane on which the filament orientation remains stuck at a value Θ can be determined explicitly by substituting (28) and (29) into $-a \le F(\Theta;\lambda_1,\lambda_2) \le a$. Figure 8 shows these regions for three values of Θ.

The associated effective energy $\overline{W}$ can be determined (to within an additive function of λ_1 and λ_2) by integrating (34). Figure 6 shows a plot of $\overline{W}$ in red (as well as W and W_ϵ in blue and black) versus Θ. The flat segments of $\overline{W}$, correspond to zero driving force, and therefore characterize where the system gets stuck. These parts of $\overline{W}$ correspond to the segments of W_ϵ that involve local minima (when $\epsilon \to 0$); see discussion in the paragraph just below (30). As noted previously, one might speak of the single local minimum Θ_{eq} (in the case without

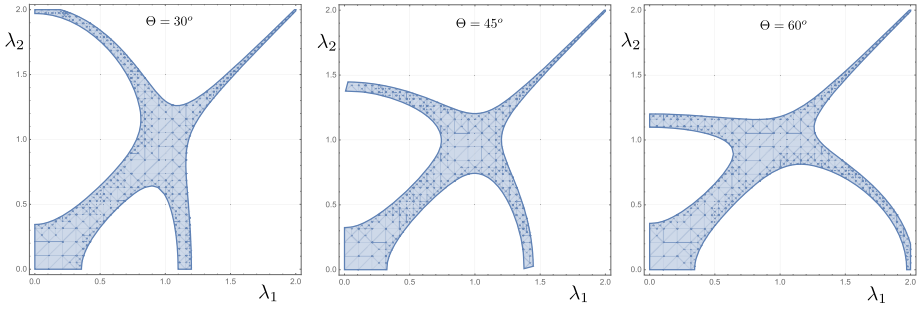

Fig. 8 The regions of the λ_1, λ_2-plane where the filament orientation remains stuck at an angle Θ. The figure has been drawn for $a = 0.1$. Our interest is particularly in the lower right quadrant where $\lambda_1 > 1$ and $0 < \lambda_2 < 1$

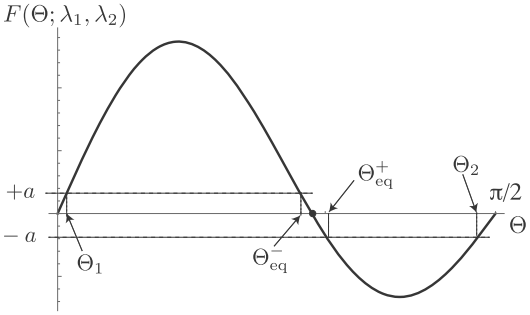

Fig. 9 Intersection of the curve corresponding to the driving force $F(\Theta; \lambda_1, \lambda_2)$ with the horizontal lines with intercept $\pm a$. The figure has been drawn in the case where each line intersects the curve twice. This is always true for sufficiently small values of a

the wiggly energy) as having bifurcated into the two local minima corresponding to $\Theta^-_{\rm eq}$ and $\Theta^+_{\rm eq}$ (see Fig. 10) or perhaps to all of the points between them.

Finally we wish to plot the effective driving force $\overline{F}(\Theta; \lambda_1, \lambda_2) = -\partial \overline{W}/\partial\Theta$ versus Θ (and compare it with the graphs of the driving forces F and F_ϵ). In order to do this, we must map the range inequalities in (34) into inequalities on Θ. This involves finding the roots $\Theta \in (0, \pi/2)$ of the pair of algebraic equations $F(\Theta; \lambda_1, \lambda_2) = \pm a$.

Figure 9 provides a graphical illustration of this task. The figure has been drawn for sufficiently small[8] a in which case each of these equations has two real roots (in $(0, \pi/2)$). The two roots of $F(\Theta; \lambda_1, \lambda_2) = +a$ have been denoted by Θ_1 and $\Theta^-_{\rm eq}$ where $0 < \Theta_1 < \Theta^-_{\rm eq} < \Theta_{\rm eq}$. Likewise $\Theta^+_{\rm eq}$ and Θ_2, with $\Theta_{\rm eq} < \Theta^+_{\rm eq} < \Theta_2 < \pi/2$, denote the two roots of $F(\Theta; \lambda_1, \lambda_2) = -a$.

From the figure we see that $F > a$ for $\Theta_1 < \Theta < \Theta^-_{\rm eq}$ and $F < -a$ for $\Theta^+_{\rm eq} < \Theta < \Theta_2$. Thus the effective driving (34) can be written as

$$\overline{F}(\Theta; \lambda_1, \lambda_2) = -\frac{\partial \overline{W}}{\partial \Theta} = \begin{cases} +\sqrt{[F(\Theta; \lambda_1, \lambda_2)]^2 - a^2}, & \Theta_1 < \Theta < \Theta^-_{\rm eq}, \\ 0, & \text{otherwise}, \\ -\sqrt{[F(\Theta; \lambda_1, \lambda_2)]^2 - a^2}, & \Theta^+_{\rm eq} < \Theta < \Theta_2. \end{cases} \tag{35}$$

[8] For larger values of a it is possible that only one of these equations has real roots or that neither has real roots. We shall restrict attention to the case where a is sufficiently small such that each equation has 2 real roots. The extension to the other cases is straightforward though (possibly) physically less interesting.

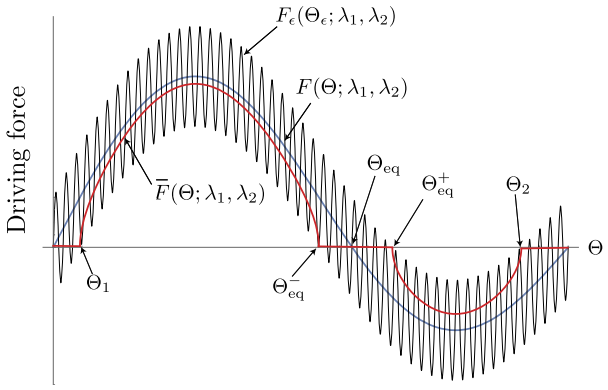

Fig. 10 Driving forces $\overline{F}$ (red), F_ϵ (black) and F (blue) versus Θ at fixed λ_1, λ_2. The figure has been drawn for $\lambda_1 = 1.5$, $\lambda_2 = 0.5$, $\epsilon = 0.005$ and $a = 0.4$

The driving forces F, F_ϵ and $\overline{F}$, are given by (28), (31) and (35) respectively and their variations with Θ are shown in Fig. 10. The system gets stuck (in a metastable configuration) in the horizontal red segments.

Finally, to illustrate all of this, consider a loading program with $\lambda_2 = 1/\lambda_1$ so that we then have only one independent loading parameter which we take to be λ_1. Using MATHEMATICA, we find that $F(\Theta;\lambda_1,\lambda_1^{-1}) > a$ in the lower shaded region of the λ_1, Θ-plane in Fig. 11, and similarly that $F(\Theta;\lambda_1,\lambda_1^{-1}) < -a$ within the upper shaded region.[9] Thus the fiber orientation remains stuck and does not evolve in the unshaded regions, evolving only if and when the loading enters a shaded region. Next, we monotonically increased the stretch λ_1 according to $\lambda_1(t) = 1+2[1-\exp(-t)]$ and solved the kinetic equation for several initial fiber orientations. The values of the initial orientations are given in the figure caption. The resulting solution trajectories, $\lambda_1(t)$, $\Theta(t)$, are shown in Fig. 11 (where the red curve corresponds to the equilibrium angle $\Theta_{\rm eq}(t)$ as given by (20) for this loading). The curves clearly show how the solution trajectory in this plane remains stuck (i.e., the fiber orientation does not change) until the trajectory enters a shaded region. Since the driving force F is $> a > 0$, in the lower shaded region, the orientation angle increases there; while the orientation angle decreases in the upper shaded region since the driving force is $< -a < 0$ there.

These results are consistent with the qualitative observation by Faust et al. [10] that there is a certain threshold of stretch that must be exceeded before fiber reorientation begins to occur. We have not found quantitative information on this threshold and the results of the present paper should be tested against further experiments.

Appendix A: The equilibrium orientation

In order to compare the equilibrium fiber angle predicted here with Livne et al.'s [17] result based on linear anisotropic elasticity, let

$$\lambda_1 = 1+\varepsilon_1, \quad \lambda_2 = 1-r\varepsilon_1. \tag{A.1}$$

In order that $\lambda_1 > 1 > \lambda_2 > 0$ one must have

$$\varepsilon_1 > 0, \quad r > 0, \quad r\varepsilon_1 < 1.$$

[9] A vertical line $\lambda_1 =$ constant, for λ_1 sufficiently large, intersects the shaded regions at four points corresponding to Θ_1, $\Theta^-_{\rm eq}$, $\Theta^+_{\rm eq}$ and Θ_2.

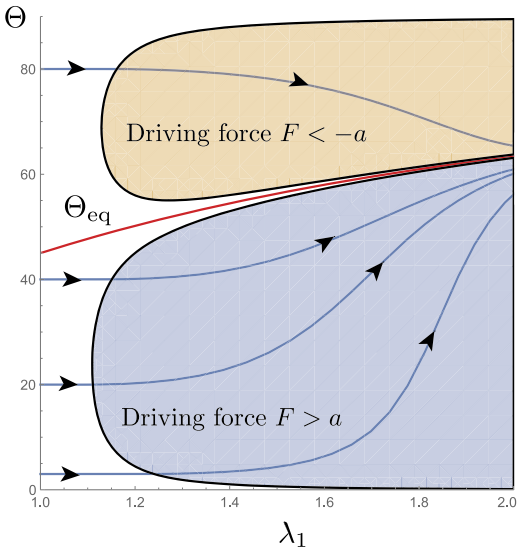

Fig. 11 The trajectories $\lambda_1(t)$, $\Theta(t)$ associated with a loading program $\lambda_1(t) = 1 + 2[1 - \exp(-t)]$, $\lambda_2(t) = 1/\lambda_1(t)$. In the unshaded region the driving force $F \in (-a, a)$: accordingly, each trajectory is initially horizontal (i.e. $\Theta(t)$ is constant) showing that the fiber orientation is stuck until the trajectory enters a shaded region. The angle can increase in the lower shaded region where the driving force $F > a > 0$ and decrease in the upper shaded region where $F < -a < 0$. The kinetic equation was solved for the initial conditions $\Theta(0) = 3^o, 20^o, 40^o$ and 80^o. The figure has been drawn for $a = 0.05$. The red curve corresponds to the equilibrium angle $\Theta_{\rm eq}(t)$ given by (20) evaluated for the loading at hand

Substituting (A.1) into (20) and (21) yields the equilibrium fiber angles

$$\cos^2\Theta_{\rm eq} = \frac{2 - r(\lambda_1 - 1)}{2 + (1 - r)(\lambda_1 - 1)}\,\frac{r}{1 + r}, \tag{A.2}$$

$$\cos^2\theta_{\rm eq} = \frac{2 - r(\lambda_1 - 1)}{2 + (1 - r)(\lambda_1 - 1)}\,\frac{r}{1 + r}\,\lambda_1^2. \tag{A.3}$$

Figure 12 shows the variation of $\cos^2\theta_{\rm eq}$ with $1/(1 + r)$ for two values of λ_1. The curves look misleadingly linear on the plotted range which they are not (unless $\lambda_1 = 1$).

Even though Livne et al. [17] report strain amplitudes up to 24%, suppose we treat $|\varepsilon_1|$ as $\ll 1$. Then the two preceding expressions can both be approximated as

$$\cos^2\Theta_{\rm eq} \approx \cos^2\theta_{\rm eq} \approx 1 - \frac{1}{1 + r}. \tag{A.4}$$

The equilibrium angle derived by Livne et al. [17] was

$$\cos^2\Theta_{\rm eq} = b - \frac{2b - 1}{1 + r}, \tag{A.5}$$

which coincides with (A.4) when $b = 1$. The graphs of $\cos^2\Theta_{\rm eq}$ versus $1/(1 + r)$ according to (A.4) and (A.5) are (exactly) straight lines.

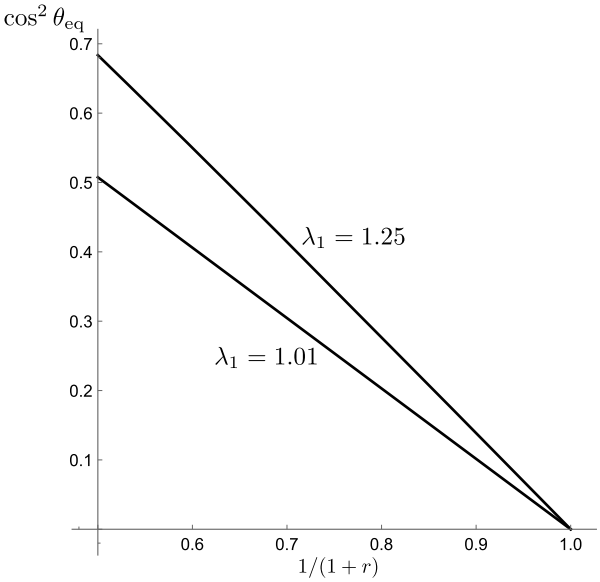

Fig. 12 Graphs of $\cos^2\theta_{\rm eq}$ versus $1/(1+r)$ according to (A.3) for two values of λ_1. The curves misleadingly look linear on the plotted range. Observe that they depend on the value of stretch λ_1 which is in contrast to the infinitesimal deformation approximation (A.4)

If we were to consider the slightly more general energy function

$$W = \frac{1}{2}\mu\Big[b(\Lambda_1^2-1)^2 + (1-b)(\Lambda_2^2-1)^2\Big], \quad \mu>0,\ 0<b\le 1, \tag{A.6}$$

that depends on both stretches Λ_1 and Λ_2, then, instead of (A.2) we obtain

$$\cos^2\Theta_{\rm eq} = \frac{2(1-b+br)+(1-b-br^2)\varepsilon_1}{2(1+r)+(1-r^2)\varepsilon_1}, \tag{A.7}$$

which upon approximation for small ε_1 leads precisely to (A.5).

Appendix B: Slow dynamic evolution

As mentioned previously, our evolution equations (27), (28), (29) coincide with equations (3.39), (4.42) of Ciambella and Nardinocchi [8]. To compare them with Livne et al. [17]'s evolution equation let

$$\lambda_1 = 1+\varepsilon_1, \quad \lambda_2 = 1+\varepsilon_2 = 1-r\varepsilon_1. \tag{B.1}$$

On substituting (B.1) into (27), (28) and approximating the result for small ε_1 we get

$$\tau\dot\Theta = 4\varepsilon_1^2(1+r)^2\left[\cos^2\Theta - \frac{r}{1+r}\right]\sin 2\Theta. \tag{B.2}$$

For the slightly more general energy function (A.6) we find

$$\tau\dot\Theta = 4\varepsilon_1^2(1+r)^2\left[\cos^2\Theta - \frac{rb+1-b}{1+r}\right]\sin 2\Theta. \tag{B.3}$$

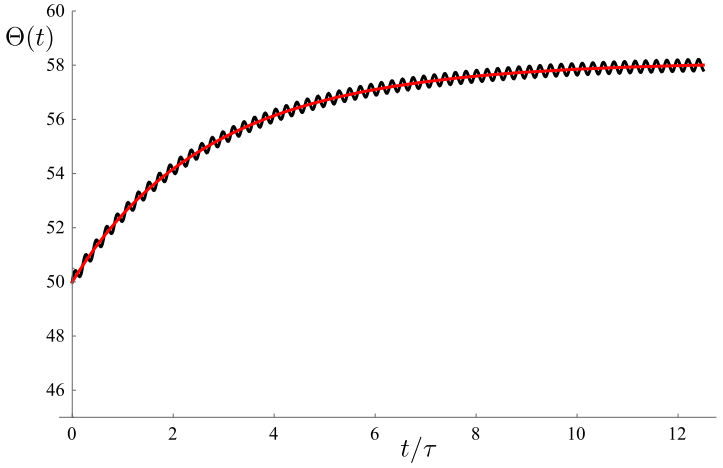

Fig. 13 Fiber orientation $\Theta(t)$ versus time t/τ. The oscillatory (black) curve corresponds to the solution of the kinetic equation (27) for the loading (B.5). The monotonic (red) curve is associated with the solution of the averaged equation (B.6). The figure has been drawn for $\tau\omega = 30$, $\varepsilon_0 = 0.1$, $\overline{\lambda}_1 = 1.2$, $\overline{\lambda}_2 = 0.9$ and $\Theta(0) = 50^\circ$

Livne et al. [17]'s formula, based on anisotropic linear elasticity, is

$$\tau\dot{\Theta} = K\varepsilon_1^2(1+r)^2\left[\cos^2\Theta - \frac{rb+1-b}{1+r}\right]\sin 2\Theta, \tag{B.4}$$

where b and K are material parameters.

Finally, consider the following loading involving periodic oscillations superposed on a bi-axial stretch:

$$\lambda_1(t) = \overline{\lambda}_1 + \varepsilon_0\cos\omega t, \quad \lambda_2(t) = \overline{\lambda}_2 + \varepsilon_0\cos\omega t. \tag{B.5}$$

Here the constant positive parameters $\overline{\lambda}_1$ and $\overline{\lambda}_2$ characterize the base state, ε_0 is the amplitude of the superposed oscillation and ω its frequency. The oscillatory (black) curve in Fig. 13 shows the variation of $\Theta(t)$ with t found by solving (27) for the loading (B.5); the underlying parameter values are given in the figure caption. The fiber orientation does not converge (strictly) to an equilibrium orientation since the loading oscillates indefinitely. Instead, it settles down to a steady oscillation about an equilibrium orientation.

If the time-scale τ of the kinetic processes is much slower than the time-scale $2\pi/\omega$ of the loading, we can average equation (27), (28) over the fast time-scale (in which calculation $\Theta(t)$ is treated as constant). This leads to

$$\tau\dot{\Theta} = \overline{F}(\Theta), \tag{B.6}$$

where the averaged driving force is

$$\overline{F}(\Theta) = \left[\overline{A}\cos^2\Theta - \overline{B}\right]\sin 2\Theta, \tag{B.7}$$

and the averaged values of A and B are

$$\overline{A} = \frac{1}{2\pi/\omega}\int_0^{2\pi/\omega} A(\lambda_1(t),\lambda_2(t))dt = (\overline{\lambda}_1 - \overline{\lambda}_2)^2\left[(\overline{\lambda}_1 + \overline{\lambda}_2)^2 + 2\varepsilon_0^2\right],$$

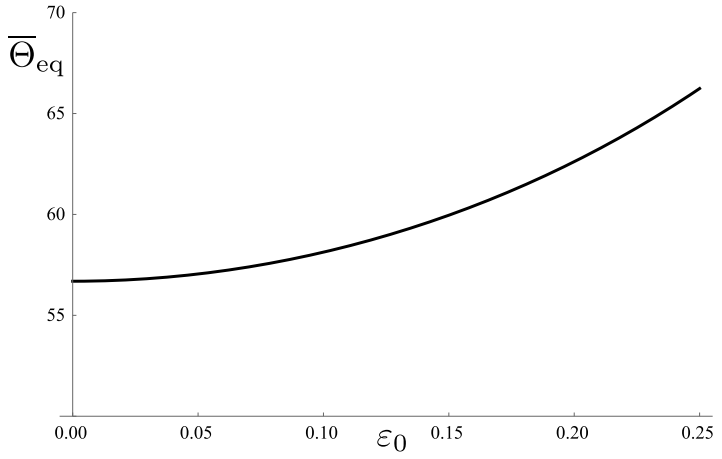

Fig. 14 The effect of the amplitude ε_0 of oscillation on the average equilibrium orientation $\overline{\Theta}_{eq}$ according to (B.8). The figure has been drawn for $\overline{\lambda}_1 = 1.2$, $\overline{\lambda}_2 = 0.9$

$$\overline{B} = \frac{1}{2\pi/\omega}\int_0^{2\pi/\omega} B(\lambda_1(t), \lambda_2(t))dt = \frac{1}{2}(\overline{\lambda}_1 - \overline{\lambda}_2)\Big[2(\overline{\lambda}_1 + \overline{\lambda}_2)(1 - \overline{\lambda}_2^2) - (\overline{\lambda}_1 + 5\overline{\lambda}_2)\varepsilon_0^2\Big].$$

The monotonic (red) curve in Fig. 13 shows a plot of $\Theta(t)$ versus t according to the averaged evolution equation (B.6), (B.7).

The average equilibrium orientation of the fibers according to the averaged equation (B.6), (B.7) is given by

$$\cos^2\overline{\Theta}_{eq} = \frac{\overline{B}}{\overline{A}} = \frac{1 - \overline{\lambda}_2^2 - (\overline{\lambda}_1 + 5\overline{\lambda}_2)(\overline{\lambda}_1 + \overline{\lambda}_2)^{-1}\varepsilon_0^2/2}{\overline{\lambda}_1^2 - \overline{\lambda}_2^2 + 2(\overline{\lambda}_1 - \overline{\lambda}_2)(\overline{\lambda}_1 + \overline{\lambda}_2)^{-1}\varepsilon_0^2}. \tag{B.8}$$

Comparing (B.8) with (20) shows how the amplitude of oscillation ε_0 affects the average equilibrium orientation. Figure 14 shows a plot of $\overline{\Theta}_{eq}$ versus ε_0 for the parameter values indicated in the caption. Clearly, (B.8) shows that the average equilibrium orientation (also) depends on the bi-axiality ratio $\overline{\lambda}_2/\overline{\lambda}_1$.

Acknowledgements R.A. and E.P. gratefully acknowledge the support of the MIT-FVG Seed Fund. The work of G.T. and E.P. was supported by the Italian PRIN 2017 project "Mathematics of active materials: From mechanobiology to smart devices" as well as by the Italian National Group of Mathematical Physics (GNFM-INdAM). G.T. acknowledges the Grant of Excellence Departments, MIUR, Italian Ministry of University and Research (Art.1, commi 314-337, Legge 232/2016).

Author contributions All authors contributed equally to this work.

Funding Note Open Access funding provided by the MIT Libraries.

Declarations

Competing interests The authors declare no competing interests.

References

1. Abeyaratne, R., Chu, C., James, J.: Kinetics of materials with wiggly energies: theory and application to the evolution of twinning microstructures in a Cu-Al-Ni shape memory alloy. Philos. Mag. A **73**(2), 457–497 (1996)
2. Abeyaratne, R., Chu, C., James, R.: Kinetics and hysteresis in martensitic single crystals. In: Proc. Symposium on the Mechanics of Phase Transformations and Shape Memory Alloys, AMD, vol. 189, pp. 85–98. ASME, New York (1994)
3. Abeyaratne, R., Knowles, J.K.: On the driving traction acting on a surface of strain discontinuity in a continuum. J. Mech. Phys. Solids **38**(3), 345–360 (1990). https://doi.org/10.1016/0022-5096(90)90003-M
4. Abeyaratne, R., Knowles, J.K.: A note on the driving traction acting on a propagating interface: adiabatic and non-adiabatic processes of a continuum. J. Appl. Mech. **67**(4), 829–830 (2000). https://doi.org/10.1115/1.1308577
5. Callen, H.: Thermodynamics and an Introduction to Thermostatistics, 2nd edn. Wiley, New York (1985)
6. Chen, B., Kemkemer, R., Deibler, M., Spatz, J., Gao, H.: Cyclic stretch induces cell reorientation on substrates by destabilizing catch bonds in focal adhesions. PLoS ONE **7**, e48346 (2012)
7. Ciambella, J., Lucci, G., Nardinocchi, P., Preziosi, L.: Passive and active fiber reorientation in anisotropic materials. Int. J. Eng. Sci. **176**, 103688 (2022). https://doi.org/10.1016/j.ijengsci.2022.103688
8. Ciambella, J., Nardinocchi, P.: Torque-induced reorientation in active fibre-reinforced materials. Soft Matter **15**(9), 2081–2091 (2019). https://doi.org/10.1039/C8SM02346H
9. De, R., Zemel, A., Safran, S.A.: Do cells sense stress or strain? Measurement of cellular orientation can provide a clue. Biophys. J. **94**, L29–L31 (2008)
10. Faust, U., Hampe, N., Rubner, W., Kirchgessner, N., Safran, S., Hoffmann, B., Merkel, R.: Cyclic stress at mhz frequencies aligns fibroblasts in direction of zero strain. PLoS ONE **6**(12), e26983 (2011). https://doi.org/10.1371/journal.pone.0028963
11. Hayakawa, K., Sato, N., Obinata, T.: Dynamic reorientation of cultured cells and stress fibers under mechanical stress from periodic stretching. Exp. Cell Res. **268**, 104–114 (2001)
12. Wang, J.H., Goldschmidt-Clermont, P., Wille, J., Yin, F.C.: Specificity of endothelial cell reorientation in response to cyclic mechanical stretching. J. Biomech. **34**, 1563–1572 (2001)
13. Jungbauer, S., Gao, H., Spatz, J., Kemkemer, R.: Two characteristic regimes in frequency-dependent dynamic reorientation of fibroblasts on cyclically stretched substrates. Biophys. J. **95**, 3470–3478 (2008)
14. Kestin, J.: A Course in Thermodynamics, vol. II. McGraw Hill, New York (1979)
15. Lazopoulos, K., Pirentis, A.: Substrate stretching and reorganization of stress fibers as a finite elasticity problem. Int. J. Solids Struct. **44**, 8285–8296 (2007)
16. Lazopoulos, K., Stamenovic, D.: A mathematical model of cell reorientation in response to substrate stretching. Mol. Cell. Biomech. **3**, 43–48 (2006)
17. Livne, A., Bouchbinder, E., Geiger, B.: Cell reorientation under cyclic loading. Nat. Commun. **5**, 3938 (2014). https://doi.org/10.1038/ncomms4938
18. Lucci, G., Giverso, C., Preziosi, L.: Cell orientation under stretch: stability of a linear viscoelastic model. Math. Biosci. **337**, 108630 (2021). https://doi.org/10.1016/j.mbs.2021.108630
19. Lucci, G., Preziosi, L.: A nonlinear elastic description of cell preferential orientations over a stretched substrate. Biomech. Model. Mechanobiol. **20**(2), 631–649 (2021). https://doi.org/10.1007/s10237-020-01406-4
20. Melnik, A.V., Goriely, A.: Dynamic fiber reorientation in a fiber-reinforced hyperelastic material. Math. Mech. Solids **18**(6), 634–648 (2013). https://doi.org/10.1177/1081286513485773
21. Ogden, R.W.: Nonlinear elasticity, material stability and residual stresses in soft tissue. In: Holzapfel, G.A., Ogden, R. (eds.) Biomechanics of Soft Tissue in Cardiovascular Systems. CISM Courses and Lecture Series, vol. 441. Springer, Berlin (2003)
22. Ristori, T., Vigliotti, A., Baaijens, F.P.T., Loerakker, S., Deshpande, V.S.: Prediction of cell alignment on cyclically strained grooved substrates. Biophys. J. **111**, 2274–2285 (2016)

23. Safran, S., De, R.: Nonlinear dynamics of cell orientation. Phys. Rev. E, Stat. Nonlinear Soft Matter Phys. **80**, 060901 (2009)
24. Vigliotti, A., Ronan, W., Baaijens, F.P.T., Deshpande, V.S.: A thermodynamically motivated model for stress-fiber reorganization (2016)